



Defect-Band Emission Photoluminescence Imaging on Multi-Crystalline Si Solar Cells

Preprint

Fei Yan, Steve Johnston,
and Mowafak Al-Jassim
National Renewable Energy Laboratory

Katherine Zaunbrecher
*National Renewable Energy Laboratory and Colorado
State University*

Omar Sidelkheir and Alain Blosse
Calisolar

*Presented at the 37th IEEE Photovoltaic Specialists Conference
(PVSC 37)
Seattle, Washington
June 19-24, 2011*

NREL is a national laboratory of the U.S. Department of Energy, Office of Energy Efficiency & Renewable Energy, operated by the Alliance for Sustainable Energy, LLC.

Conference Paper
NREL/CP-5200-50725
July 2011

Contract No. DE-AC36-08GO28308

NOTICE

The submitted manuscript has been offered by an employee of the Alliance for Sustainable Energy, LLC (Alliance), a contractor of the US Government under Contract No. DE-AC36-08GO28308. Accordingly, the US Government and Alliance retain a nonexclusive royalty-free license to publish or reproduce the published form of this contribution, or allow others to do so, for US Government purposes.

This report was prepared as an account of work sponsored by an agency of the United States government. Neither the United States government nor any agency thereof, nor any of their employees, makes any warranty, express or implied, or assumes any legal liability or responsibility for the accuracy, completeness, or usefulness of any information, apparatus, product, or process disclosed, or represents that its use would not infringe privately owned rights. Reference herein to any specific commercial product, process, or service by trade name, trademark, manufacturer, or otherwise does not necessarily constitute or imply its endorsement, recommendation, or favoring by the United States government or any agency thereof. The views and opinions of authors expressed herein do not necessarily state or reflect those of the United States government or any agency thereof.

Available electronically at <http://www.osti.gov/bridge>

Available for a processing fee to U.S. Department of Energy and its contractors, in paper, from:

U.S. Department of Energy
Office of Scientific and Technical Information

P.O. Box 62
Oak Ridge, TN 37831-0062
phone: 865.576.8401
fax: 865.576.5728
email: <mailto:reports@adonis.osti.gov>

Available for sale to the public, in paper, from:

U.S. Department of Commerce
National Technical Information Service
5285 Port Royal Road
Springfield, VA 22161
phone: 800.553.6847
fax: 703.605.6900
email: orders@ntis.fedworld.gov
online ordering: <http://www.ntis.gov/help/ordermethods.aspx>

Cover Photos: (left to right) PIX 16416, PIX 17423, PIX 16560, PIX 17613, PIX 17436, PIX 17721



Printed on paper containing at least 50% wastepaper, including 10% post consumer waste.

DEFECT-BAND EMISSION PHOTOLUMINESCENCE IMAGING ON MULTI-CRYSTALLINE Si SOLAR CELLS

Fei Yan¹, Steve Johnston¹, Katherine Zaunbrecher^{1,2}, Mowafak Al-Jassim¹, Omar Sidelkheir³, and Alain Blosse³

¹National Renewable Energy Laboratory, Golden, CO 80401, U.S.A.

²Colorado State University, Fort Collins, CO 80523, U.S.A.

³Calisolar, Sunnyvale, CA 94085, U.S.A

ABSTRACT

Defect-band photoluminescence (PL) imaging with an InGaAs camera was applied to multicrystalline silicon (mc-Si) wafers, which were taken from different heights of different Si bricks. Neighboring wafers were picked at six different processing steps, from as-cut to post-metallization. By using different cut-off filters, we were able to separate the band-to-band emission images from the defect-band emission images. On the defect-band emission images, the bright regions that originate from the grain boundaries and defect clusters were extracted from the PL images. The area fraction percentage of these regions at various processing stages shows a correlation with the final cell electrical parameters.

INTRODUCTION

Different imaging techniques have been developed recently and turned into rapid and nondestructive inline characterization tools. Electroluminescence (EL) imaging collects the light coming out from finished solar cells under forward bias [1-5]. Spatially resolved information about the recombination, resistance, and cracks can be obtained in seconds. Therefore, EL imaging has been widely used not only on finished cells, but also on assembled modules. Reverse-bias EL (ReBEL) imaging has been used to study the reverse breakdown behavior on different solar cells [6-10]. However, because EL imaging requires electrical contacts, it is limited to use on the finished solar cells and any steps thereafter. PL imaging uses optical excitation to generate electron-hole pairs and a camera detects the radiative recombination emission [11, 12]. It has a great advantage as a contactless technique and can be applied to essentially all processing steps, from the silicon ingots and bricks to all processing steps on the wafer scale. A lot of work has been done on the band-to-band emission around 1150 nm using Si-CCD cameras, which gives great information about the defects and dislocation clusters inside the silicon wafers. Several papers have been published on mapping the defect-band luminescence at around 1550 nm [13-16], which corresponds to the factors which limit the final cell's efficiency.

EXPERIMENT

In this paper, we used an InGaAs camera to quickly image the defect-band emission and studied the defect-band PL images on 156 mm x 156 mm mc-Si wafers that had gone

through six processing steps, including as-cut, texturing, emitter diffusion, phosphosilicate glass (PSG) removal, anti-reflection coatings (ARC) deposition and metallization. These wafers were selected from different bricks at different heights, including near the bottom, in the middle and near the top. We had 30 wafers from each step. We examined a total of 180 wafers, which give us enough data points for a statistical analysis.

We used a FLIR SC2500 NIR InGaAs Camera (320 x 256 pixels) with a StingRay 25 mm wide angle lens for defect-band PL imaging. The detection sensitivity of the InGaAs camera is in the 0.9 to 1.7 μm range, which covers both the band-to-band emission at ~ 1.1 eV and the defect-related emission at ~ 0.8 eV from silicon, as shown in Fig. 1. The optical excitation source used for PL imaging is composed of four 30 W, 810 nm laser diodes coupled to optical fibers. The fibers are then coupled to collimators and engineered diffusers. They emit from opposite angles to provide uniform excitation over the area of the sample. All PL imaging work is done at a condition close to 1 sun intensity. To block reflected light from the sample and stage area, RG1000 Schott glass filters are mounted to the camera lens. To separate the band-to-band emission and defect-related emission, different cut-off filters were mounted to the lens.

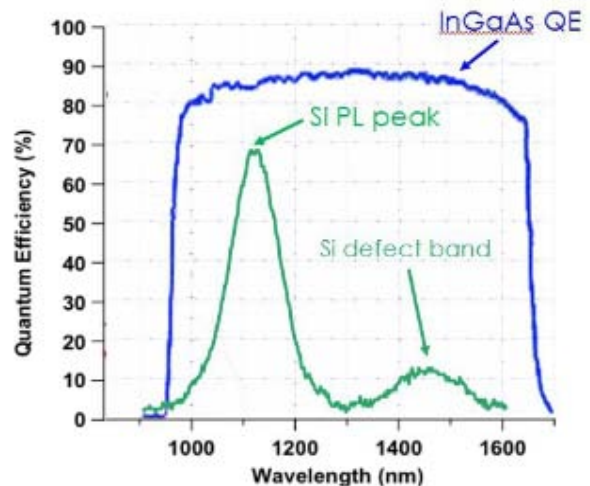


Figure 1 Quantum efficiency curve of the Near-IR InGaAs camera and the PL curve of a Si sample with both band-to-band PL peak and defect-band shown.

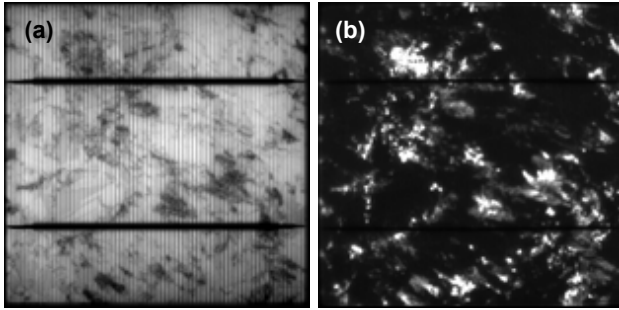


Figure 2 PL imaging of mc-Si solar cell comparing (a) band-to-band emissions to (b) defect-band emissions when using a 1350 nm long-pass filter.

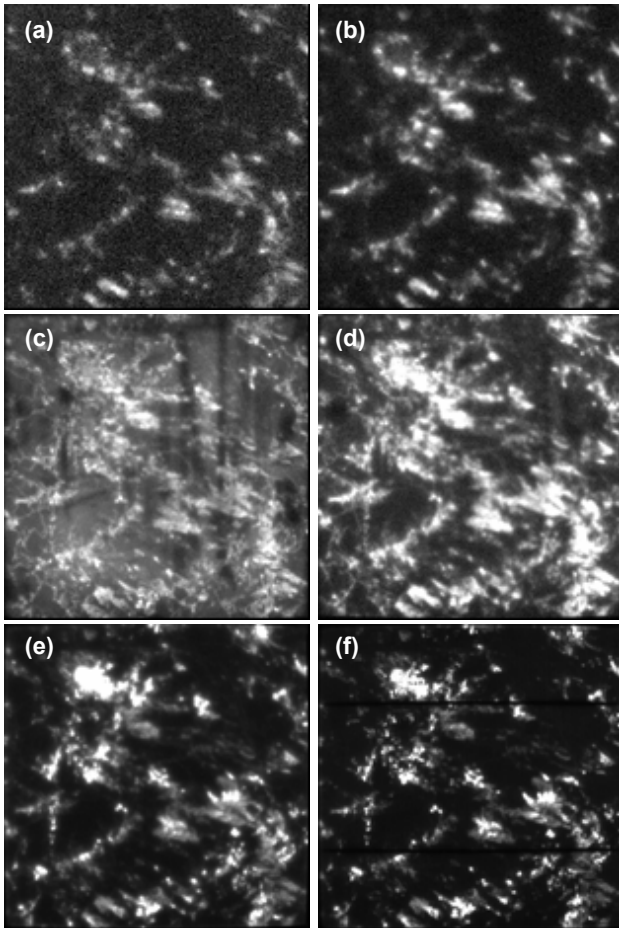


Figure 3 Defect-band emission PL images on wafers after six different processing steps: (a) as-cut, (b) texturing, (c) emitter diffusion, (d) PSG removal, (e) ARC deposition, and (f) metallization.

Fig. 2 shows a comparison of the band-to-band emission and defect-band-emission PL images on a mc-Si finished cell. Most of the regions that are dark in the band-to-band emission image Fig. 2(a) have sub-bandgap radiative

emissions and are predominantly bright in the defect-band emission image Fig. 2(b).

Defect-band emission PL images on six neighboring wafers from various processing steps are shown in Fig. 3. The same defect pattern persists from the beginning to the end. The as-cut and post-texturing wafers have a relatively weak PL signal due to the surface recombination, which can also be observed in the band-to-band PL images (not shown here). After emitter diffusion and PSG removal, wafers have a stronger PL signal but the contrast is not the best. After ARC and metallization steps, the defect-band PL images have an excellent signal and contrast. One may notice that through these six processing steps, the relative intensity of some bright regions changes. For an example, near the top-left corner of Fig. 3(a) and (b), there is a big cluster with grey defect PL. Later after the following processing steps, this cluster becomes really bright with a very strong defect PL emission. The cause of this change is not totally understood at this moment.

The size of the dislocation clusters grows along the direction of the solidification of the ingot, which is consistent with the band-to-band PL images we took on bricks (not shown here). Near the bottom of the brick, we observed a small fraction of the area with defect-band emission as shown in Fig. 4(a). The defect clusters become much bigger at the middle of the brick and almost dominates the whole wafer at the top of the brick. The efficiencies of these finished cells show a gradient decrease from the bottom to the top. This nice trend can be further quantified by counting the area fraction of the defect area over the whole wafer area.

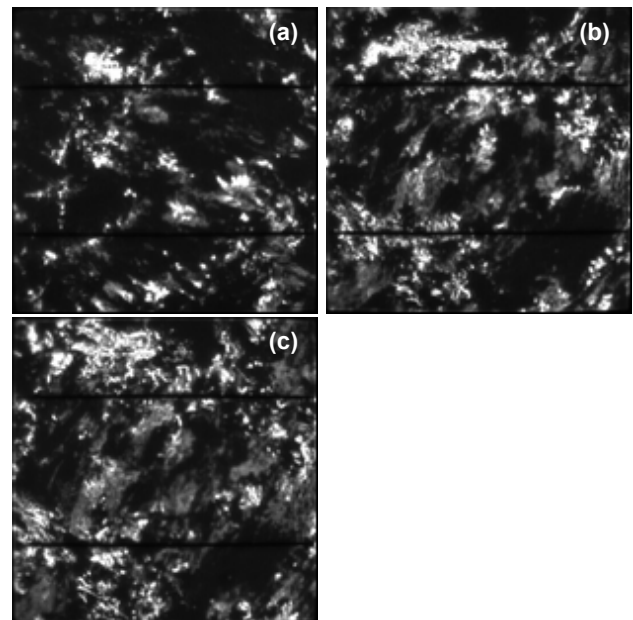


Figure 4 Defect-band emission PL images on wafers from different height of a brick: (a) near bottom, (b) middle, and (c) near top.

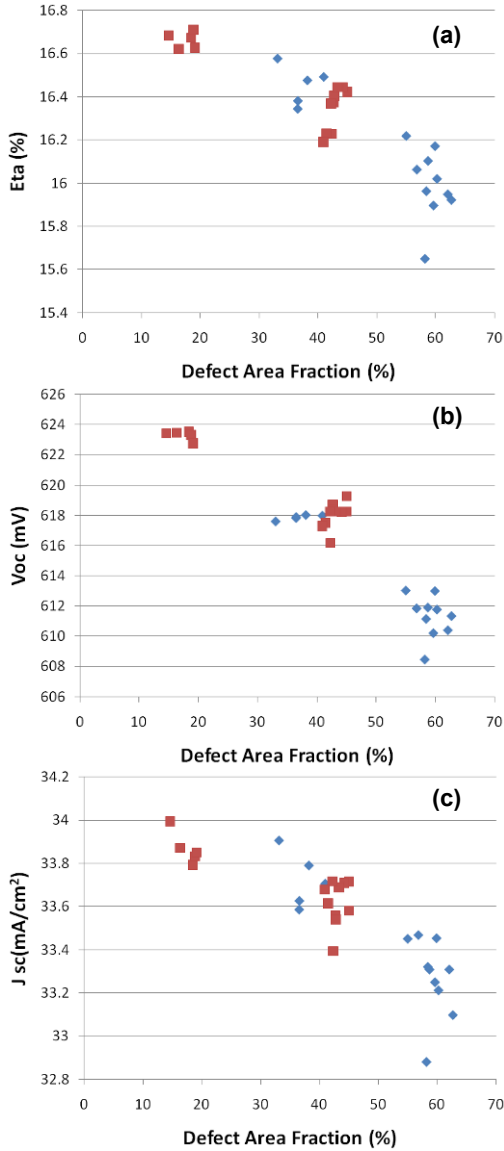


Figure 5 Defect area percentage from InGaAs PL images of the finished cell vs. solar cell (a) efficiency (b) V_{oc} and (c) J_{sc} .

On all the 30 wafers from each step, we used the same threshold to highlight the bright defect regions. The count of image pixels above this threshold compared to the total number of pixels in an image gives a defect area fraction for each wafer. We correlated the defect percentage from each step with the finished cell's parameters, including efficiency, open-circuit voltage (V_{oc}) and short-circuit current (J_{sc}). An example of the correlation using the InGaAs PL images from the finished cells is shown in Fig. 5. A linear correlation is clearly visible on all three plots. The variations of these parameters are about 1% absolute in final cell efficiency, 15 mV absolute in V_{oc} , and 1 mA/cm² absolutely in J_{sc} .

Similar correlation was seen using defect-band PL images from wafers after other processing steps. Fig. 6 shows the efficiency correlation from as-cut, post-PSG removal and post-ARC wafers. The correlations with V_{oc} and J_{sc} still hold but are not shown here. It is especially interesting to see the correlation on the as-cut wafers, because it demonstrates that this defect PL imaging technique can be applied on the starting as-cut wafers. Final cell efficiencies can be predicted based on defect PL images on the as-cut wafers. Incoming wafers can also be sorted and sent to different specially designed processing lines to optimize the final cells performance.

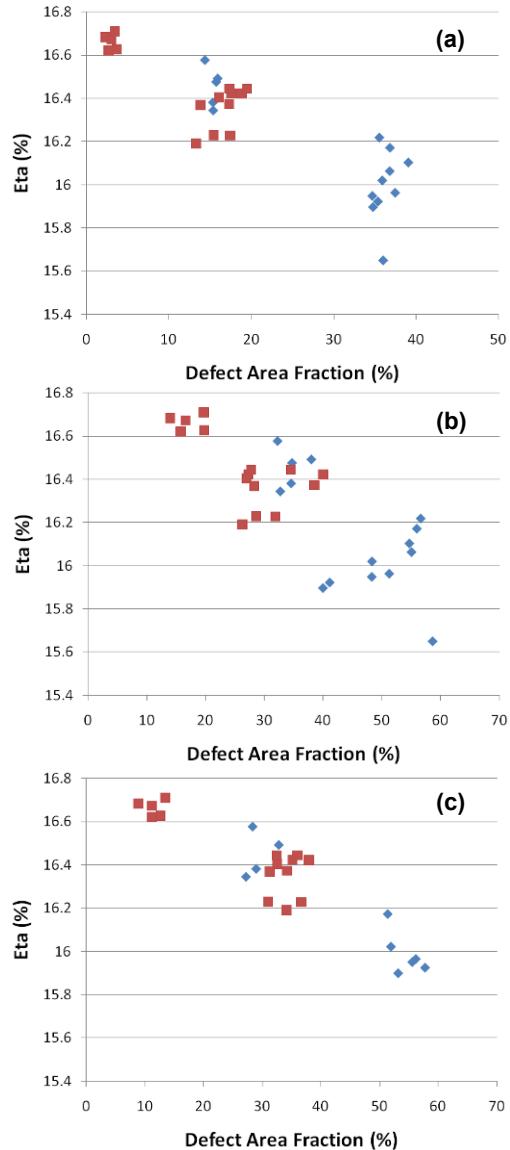


Figure 6 Defect area percentage from (a) as-cut, (b) post-PSG removal, and (c) post-ARC vs. finished cell efficiency.

SUMMARY

PL imaging with an InGaAs camera was used to study mc-Si wafers from partially processed to finished solar cells. By mounting different short-pass and long-pass cut-off filters, we were able to separate the band-to-band emission PL signal from the defect-band emission PL signal. The dark areas on the band-to-band images are correspondingly bright on the defect-band PL images due to the defect-related emission at ~1550 nm from silicon. By setting a threshold on these images, we can get an area fraction of the bright areas on each defect-band emission image. These area percentages were plotted against efficiency, V_{OC} and J_{SC} . Good correlations on these plots after different processing steps suggest that defect-band emission PL imaging could be applied as a promising technique for inline material monitoring and process control.

ACKNOWLEDGEMENT

This work was supported by the U.S. Department of Energy under Contract No. DE-AC36-08GO28308 with the National Renewable Energy Laboratory. and with support from the American Recovery and Reinvestment Act of 2009.

REFERENCES

- [1] T. Fuyuki, H. Kondo, T. Yamazaki, Y. Takahashi, and Y. Uraoka, "Photographic Surveying of Minority Carrier Diffusion Length in Polycrystalline Silicon Solar Cells by Electroluminescence", *Appl. Phys. Lett.* **86**, 2005, pp. 262108.
- [2] T. Fuyuki, H. Kondo, Y. Kaji, A. Ogane, and Y. Takahashi, "Analytic Findings in the Electroluminescence Characterization of Crystalline Silicon Solar Cells", *J. Appl. Phys.* **101**, 2007, pp. 023711.
- [3] P. Wurfel, T. Trupke, T. Puzzer, E. Schaffer, W. Warta, and S. W. Glunz, "Diffusion Lengths of Silicon Solar Cells from Luminescence Images", *J. Appl. Phys.* **101**, 2007, pp. 123110.
- [4] T. Kirchartz and U. Rau, "Electroluminescence Analysis of High Efficiency Cu(In,Ga)Se₂ Solar Cells", *J. Appl. Phys.* **102**, 2007, pp. 104510.
- [5] U. Rau, T. Kirchartz, A. Helbig, and B. E. Pieters, "Electroluminescence Imaging of Cu(In,Ga)Se₂ Thin Film Solar Modules", *2009 Spring MRS Meeting*, San Francisco, CA, April pp. 13-17.
- [6] A. G. Chynoweth and K. G. McKay, "Photon Emission from Avalanche Breakdown in Silicon", *Physical Review* **102**, 1956, pp. 369-376.
- [7] M. Morschbach, M. Oehme, and E. Kasper, "Visible Light Emission by a Reverse-Biased Integrated Silicon Diode", *IEEE Trans. Elec. Dev.* **54**, 2007, pp. 1091-1094.
- [8] M. Kasemann et al., "Spatially Resolved Silicon Solar Cell Characterization using Infrared Imaging Methods", *33rd IEEE PVSC*, 2008, pp. 148.
- [9] D. Lausch, K. Petter, H. von Wenckstern, and M. Grundmann, "Correlation of Pre-Breakdown Sites and Bulk Defects in Multicrystalline Silicon Solar Cells", *Phys. Status Solidi RRL* **3**, 2009, pp. 70-72.
- [10] M. Schneemann, A. Helbig, T. Kirchartz, R. Carius, and U. Rau, "Reverse biased electroluminescence spectroscopy of crystalline silicon solar cells with high spatial resolution," *phys. stat. sol. (a)* **207**, 2010, pp. 2597-2600.
- [11] T. Trupke, R. A. Bardos, M. D. Abbott, F. W. Chen, J. E. Cotter, and A. Lorenz, "Fast Photoluminescence Imaging of Silicon Wafers", *32nd IEEE PVSC and WCPEC-4*, 2006, pp. 928-931.
- [12] T. Trupke, R. A. Bardos, M. C. Schubert, and W. Warta, "Photoluminescence Imaging of Silicon Wafers", *Appl. Phys. Lett.* **89**, 2006, pp. 044107.
- [13] Y. Koshka, S. Ostapenko, I. Tarasov, S. McHugo, and J. P. Kalejs, "Scanning room-temperature photoluminescence in polycrystalline silicon," *Appl. Phys. Lett.* **74** 1999, pp. 1555-1557.
- [14] I. Tarasov, S. Ostapenko, C. Haessler, and E. U. Reisner, "Spatially resolved defect diagnostics in multicrystalline silicon for solar cells," *Mat. Sci. & Engr. B* **71**, 2000, pp. 51-55.
- [15] M. Kittler, W. Seifert, T. Arguirov, I. Tarasov, and S. Ostapenko, "Room-temperature luminescence and electron-beam-induced current (EBIC) recombination behaviour of crystal defects in multicrystalline silicon," *Sol. Energy Mater. Sol. Cells* **72** , 2002, pp. 465-472.
- [16] M. Inoue, H. Sugimoto, M. Tajima, Y. Ohshita, and A. Ogura, "Microscopic and spectroscopic mapping of dislocation-related photoluminescence in multicrystalline silicon wafers," *J Mater Sci: Mater Electron* **19**, 2008, pp. 132-134.